Heliyon 6 (2020) e05149

Contents lists available at ScienceDirect

Heliyon

journal homepage: www.cell.com/heliyon

Research article

Down-regulation of COX-2 activity by 1α,25(OH)$_2$D$_3$ is VDR dependent in endothelial cells transformed by Kaposi's sarcoma-associated herpesvirus G protein-coupled receptor

Cinthya Tapia [a,b], Fernando Zamarreño [c], Gabriela Alejandra Salvador [b,d], Cecilia Irene Casali [e,f], Juan Viso [c], María del Carmen Fernandez [e,f], John H. White [g,h], Verónica González-Pardo [a,b,*]

[a] Instituto de Ciencias Biológicas y Biomédicas del Sur (INBIOSUR), Consejo Nacional de Investigaciones Científicas y Técnicas (CONICET), Bahía Blanca, Argentina
[b] Departamento de Biología, Bioquímica y Farmacia-Universidad Nacional del Sur (UNS), Argentina
[c] Instituto de Física del Sur (IFISUR), Departamento de Física, Universidad Nacional del Sur (UNS), CONICET, Bahía Blanca, Argentina
[d] Instituto de Investigaciones Bioquímicas de Bahía Blanca (INIBIBB), Consejo Nacional de Investigaciones Científicas y Técnicas (CONICET), Bahía Blanca, Argentina
[e] Universidad de Buenos Aires, Facultad de Farmacia y Bioquímica, Departamento de Ciencias Biológicas, Cátedra de Biología Celular y Molecular, Buenos Aires, Argentina
[f] Universidad de Buenos Aires, Consejo Nacional de Investigaciones Científicas y Técnicas, Instituto de Química y Fisicoquímica Biológicas Prof. Dr. Alejandro C. Paladini (IQUIFIB)-Facultad de Farmacia y Bioquímica, Buenos Aires, Argentina
[g] Department of Physiology, McGill University, Montreal, Quebec, Canada
[h] Department of Medicine, McGill University, Montreal, Quebec, Canada

ARTICLE INFO

Keywords:
1α,25(OH)$_2$D$_3$
VDR
COX-2
Kaposi's sarcoma
Biocomputational method
Biochemistry
Cancer research
Toxicology
Oncology

ABSTRACT

Our previous reports showed that 1α,25-dihydroxyvitamin D$_3$ (1α,25(OH)$_2$D$_3$) has antiproliferative actions in endothelial cells stably expressing viral G protein-coupled receptor (vGPCR) associated with the pathogenesis of Kaposi's sarcoma. It has been reported that COX-2 enzyme, involved in the tumorigenesis of many types of cancers, is induced by vGPCR. Therefore, we investigated whether COX-2 down-regulation is part of the growth inhibitory effects of 1α,25(OH)$_2$D$_3$. Proliferation was measured in presence of COX-2 inhibitor Celecoxib (10–20 μM) revealing a decreased in vGPCR cell number, displaying typically apoptotic features in a dose dependent manner similarly to 1α,25(OH)$_2$D$_3$. In addition, the reduced cell viability observed with 20 μM Celecoxib was enhanced in presence of 1α,25(OH)$_2$D$_3$. Remarkably, although COX-2 mRNA and protein levels were up-regulated after 1α,25(OH)$_2$D$_3$ treatment, COX-2 enzymatic activity was reduced in a VDR-dependent manner. Furthermore, an interaction between COX-2 and VDR was revealed through GST pull-down and computational analysis. Additionally, high-affinity prostanoid receptors (EP3 and EP4) were found down-regulated by 1α,25(OH)$_2$D$_3$. Altogether, these results suggest a down-regulation of COX-2 activity and of prostanoid receptors as part of the antineoplastic mechanism of 1α,25(OH)$_2$D$_3$ in endothelial cells transformed by vGPCR.

1. Introduction

Kaposi's sarcoma (KS) is an angioproliferative disorder of vascular endothelium and an AIDS-defining malignancy. KS Herpesvirus (KSHV or human herpesvirus-8) is the etiologic agent and Kaposi's sarcoma-associated herpesvirus G protein-coupled receptor (vGPCR) is one of the viral molecules from the lytic phase able to induce KS-associated cellular modifications through paracrine oncogenesis [1, 2, 3]. *In vivo* vGPCR induces angiogenic lesions similar to those developed in KS patients, showing powerful transforming properties [4]. Thus, vGPCR signaling pathway is of great interest for KS treatment.

KSHV- infected human dermal microvascular endothelial cells showed high expression of cyclooxygenase-2 (COX-2) [5, 6]. Shelby and collaborators have reported increased COX-2 expression in primary endothelial cells induced by vGPCR [7]. COX-2 catalyzes the conversion of arachidonic acid to Prostaglandin H2 (PGH$_2$) and, therefore, is the responsible for the generation of prostaglandins (PGs), including Prostaglandin E$_2$ (PGE$_2$), a proliferation and inflammation-activating agent [8]. COX-2 enzyme is up-regulated by mitogenic and inflammatory stimuli, exerts pro-angiogenic and anti-apoptotic properties [9, 10], and contributes to angiogenic progression of several cancers [10, 11]. Therefore, it is considered as a potential therapeutic target for preventing

* Corresponding author.
E-mail address: vgpardo@criba.edu.ar (V. González-Pardo).

https://doi.org/10.1016/j.heliyon.2020.e05149
Received 15 May 2020; Received in revised form 6 July 2020; Accepted 29 September 2020

and treating many types of malignancies [11, 12]. Moreover, COX-2 overexpression is associated with increased levels of prostanoids in tumors, which exert their biological effects through GPCRs [12]. There are four distinct E-type prostanoid EP receptors [13]; EP_3 and EP_4 represent high-affinity receptors, whereas EP_1 and EP_2 require significantly higher levels of PGE_2 for activation [14].

The active form of Vitamin D, $1\alpha,25(OH)_2D_3$, is a steroid hormone that plays a key role in calcium homeostasis. In addition, it has non-classical effects in neoplastic cells by acting as an antiproliferative, pro-apoptotic and pro-differentiating agent [15, 16]. Likewise, $1\alpha,25(OH)_2D_3$ exerts anti-inflammatory properties through the inhibition of pro-inflammatory cytokines and NF-κB signaling. Most of its actions depend on VDR, the vitamin D nuclear receptor [17]. NF-κB pathway is highly activated by vGPCR and we have shown that $1\alpha,25(OH)_2D_3$ promotes NF-κB inhibition, consequently, apoptosis is induced in endothelial cells that express vGPCR [18, 19]. It is known that inflammation promotes cancer development and $1\alpha,25(OH)_2D_3$ has shown anti-inflammatory properties in the carcinogenic microenvironments of prostate, breast, colon and ovarian cancers [17, 20]. Since COX-2 is induced in endothelial cells via vGPCR signaling [7], we investigated if this key enzyme involved in the inflammatory response is down-regulated by $1\alpha,25(OH)_2D_3$ as part of its mechanism of action.

2. Materials and methods

2.1. Chemicals and reagents

$1\alpha,25(OH)_2D_3$, and the antibiotic G418 were from Sigma-Aldrich (St. Louis, MO, USA). Puromycin was provided by Invivogen (San Diego, CA, USA). The antibodies used were rat monoclonal anti-VDR (Affinity Bioreagents, Golden, CO, USA); mouse monoclonal anti-COX-2, anti-mouse and anti-rat horseradish peroxidase–conjugated secondary antibody (Santa Cruz, CA, USA). Roche Applied Science (Indianapolis, IN, USA) provided high Pure RNA Isolation Kit. Immobilon P (polyvinylidene difluoride; PVDF) membranes were from Thermo Scientific (Rockford, IL, USA); PCR primers for mouse *Gapdh*, *Cox-2*, *EP1, EP2, EP3* and *EP4* were synthetized by Invitrogen (Thermo Scientific Inc., Rockford, IL, USA). Celecoxib (Santa Cruz, CA, USA). COX-2 Activity Assay kit (Cayman N° 760151) was from Cayman Chemical Company (Michigan, USA).

2.2. Cell lines and transfections

SV-40-immortalized murine endothelial cells stably expressing vGPCR full length receptor (vGPCR), were utilized as the experimental model of Kaposi's sarcoma previously described [21] and were kindly donated by Dr. J. Silvio Gutkind (UCSD, San Diego, California, US). vGPCR promotes tumor formation in immune-suppressed mice and induces angiogenic lesions similar to those developed in Kaposi's sarcoma when stably overexpressed [4, 21]. The expression of vGPCR was routinely verified by qRT-PCR. 500 μg mL^{-1} G418 were used to the selection of transfected cells. Previously, by transduction of lentiviral particles, stable vGPCR endothelial cells targeted with small hairpin RNA against mouse VDR (vGPCR-shVDR) or control shRNA (vGPCR-shctrl) were obtained and selected with 2 μg mL^{-1} of puromycin [21]. Cells were discarded after passage 10 andmedium was freshly changed every other day. By Western blot analysis the VDR knock-down was monitored.

2.3. Proliferation assays

vGPCR cells were cultured in 24-well plates, at a density of 4500 cells per well. After overnight growth, the cells were starvedand then treated with $1\alpha,25(OH)_2D_3$ (10 nM) or Celecoxib (10 or 20 μM) or control (vehicle, 0.1% ethanol) in triplicate in DMEM 2% FBS for 48 h. Cells were then counted in a Neubauer chamber. Dead cells were excluded using trypan blue solution at 0.4%.

2.4. MTS assays

vGPCR cells were seeded in 96-well plates at 1000 cells per well. After overnight growth, cells were starved for 24 h and then treated with $1\alpha,25(OH)_2D_3$ (10 nM) or Celecoxib (10 μM) or vehicle (0.01% ethanol) in triplicate in DMEM 2% FBS for 48 h. CellTiter 96® Aqueous one solution cell proliferation assay containing 3-(4,5-dimethylthiazol-2-yl)-5-(3-carboxymethoxyphenyl)-2- (4-sulfophenyl)-2H-tetrazolium, inner salt (MTS) was used to determine cell proliferation according to the manufacturer's instructions. Absorbance was measured at 490 nm.

2.5. COX-2 activity assay

COX activity was measured by COX-2 Activity Assay kit (Cayman N° 760151) following the recommendations provided by the manufacturer. In time response-experiments protein content from whole cell lysates was determined by the Bradford procedure to standardize the signal detected [22]. The product of the reaction was colorimetrically measured at 590 nm.

2.6. GST pull-down assay

To identify the interaction between COX-2 and VDR *in vitro*, glutathione-S-transferase expression vectors were used. BL21 *E. coli* transformed with PGEX4T3-GST or PGEX4T3-GST-VDR constructs were induced to express GST or GST-VDR fusion proteins with 400 μM isopropyl β-D-thiogalactopyranoside [23, 24]. BL21 cells were centrifuged and resuspended in 1 ml lysis buffer (20 mM Tris-HCl, pH 7.5, 100 mM NaCl, 0.5 mM EDTA, 0.5% NP-40, 3 μg/ml lysozyme and protease inhibitors). The lysate was sonicated and pelleted by centrifugation for 10 min at 10000 rpm. Equal amounts of fusion proteins quantified by Bradford procedure were incubated with glutathione-Sepharose beads for 2 h with rotation at room temperature. After a centrifugation at 500 g for 5 min the supernatant was discarded and the pellet containing glutathione-Sepharose beads plus GST or GST-VDR was added to the soluble fraction of vGPCR cell lysates and incubated for 2 h rotation at room temperature. Beads were pelleted by centrifugation and eluted by adding loading buffer for Western blot assay [25].

2.7. SDS-PAGE and Western blot

By the Bradford procedure the protein content from whole cell lysates was determined [22]. Proteins were resolved with SDS–PAGE and Western blot analyses were effected as reported before [22]. Antibodies used include monoclonal mouse anti-COX-2 (1:500), rat anti-VDR (1:6000), anti-mouse (1:5000) or anti-rat (1:5000) horseradish peroxidase-conjugated secondary antibodies.

2.8. Quantitative real-time PCR

First, total RNA was isolated using the High Pure RNA Isolation Kit (Roche). Then, RNA (0.5–1μg) reverse transcription was performed using the kit High Capacity cDNA RT (Applied biosystem). qRT-PCR reactions were performed on 5–10 ng of the resulting cDNA in an ABI 7500 Real Time PCR system (Applied Biosystems, CA, USA). Specific primers to detect *Cox-2*, *EP1, EP2, EP3* and *EP4* levels were used. Analysis of the real time PCR data was executed by the 2-delta delta Ct method using *Gapdh* as reference parameter [26]. Reactions were carried out using the SYBR

Table 1. pdb structures for rat and mouse.

	Rat	Mouse
VDR	1RJK	Modeled
COX-2	Modeled	3QMO

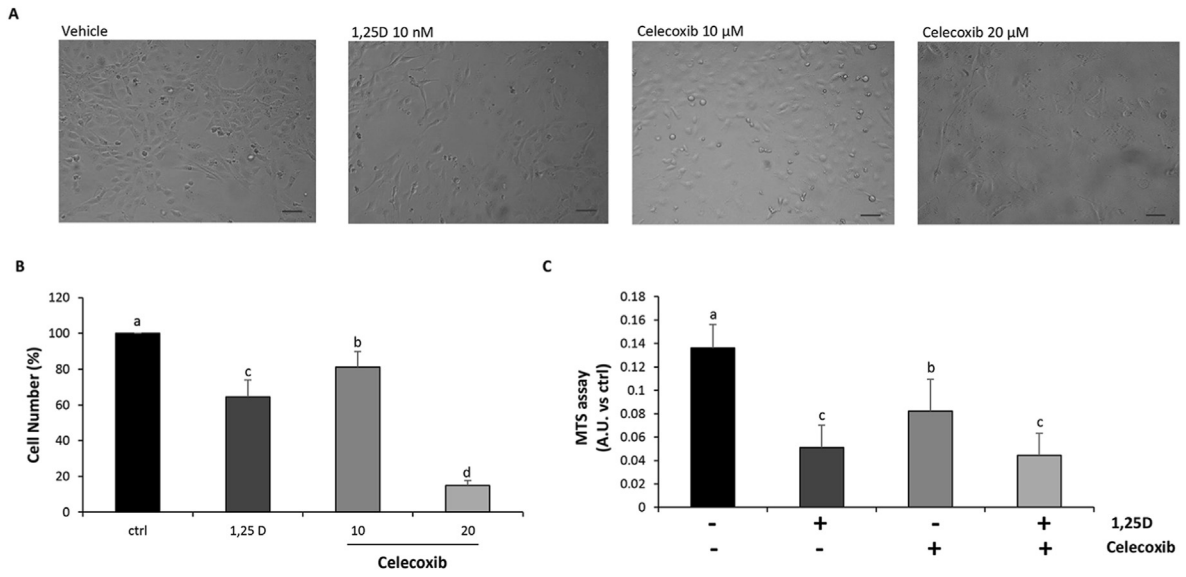

Figure 1. ***Inhibition of vGPCR cell growth by Celecoxib or 1α,25(OH)$_2$D$_3$.*** vGPCR cells were cultured and treated with 1α,25(OH)$_2$D$_3$ (1,25D) (10 nM) or Celecoxib (10–20 μM) or vehicle (0.01% ethanol) (A) and (B) or 1α,25(OH)$_2$D$_3$ (1,25D) (10 nM) or Celecoxib (10 μM) or vehicle (0.01% ethanol) (C) in DMEM 2% FBS for 48 h. A) Representative micrographs obtained by phase contrast microscopy, bar: 30 μm, magnification 200x. B) Cells were counted in Neubauer chamber. C) MTS assay was performed. Results from at least three independent experiments, were presented in bar graphs. The statistical analysis was performed by one-way ANOVA followed by the Bonferroni test. Significant differences are indicated by different letters ($p < 0.01$).

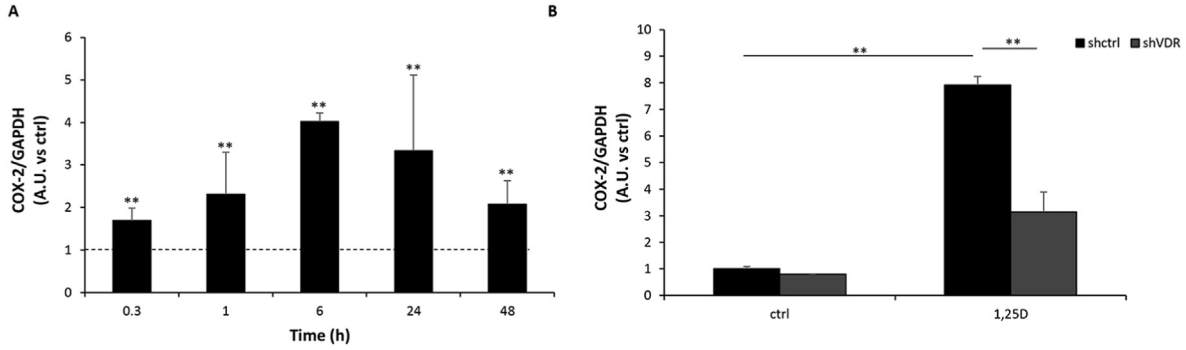

Figure 2. ***COX-2 mRNA rise is VDR dependent.*** vGPCR cells were cultured and treated with 1α,25(OH)$_2$D$_3$ (10 nM) or vehicle (0.01% ethanol) at different times (0.3–48 h) (A) or stable vGPCR cells vGPCR-shVDR or control shRNA (vGPCR-shctrl) were treated with 1α,25(OH)$_2$D$_3$ (10 nM) or vehicle (0.01% ethanol) for 24 h (B); in presence of DMEM 2% FBS. 1 μg of total RNA was extracted, reverse transcribed and gene expression of *COX-2* and *Gapdh* was assessed by qRT-PCR analysis. Data are expressed as a ratio between treated and vehicle samples at each time point and normalized to *Gapdh* mRNA levels. Data statistical significance from at least three independent experiments was evaluated using Student's t-test (**$p < 0.01$) (A). Differences between control and treated conditions in vGPCR-shctrl or -shVDR group and also treated conditions between vGPCR-shctrl and -shVDR were evaluated by Student's t-test (**$p < 0.01$) (B).

Green PCR Master Mix reagent (Applied biosystem). The primers sequences used were:

Cox-2 forward: 5′- TAGCAGATGACTGCCCAACT -3′
Cox-2 reverse: 5′- CAGGGATGAACTCTCTCCGT -3′,
EP1 (Ptgdr1) forward: 5′- CTAACCAAGAGTGCCTGGGA -3′
EP1 (Ptgdr1) reverse: 5′- GCTTCTGGGCACATTCAGAG -3′
EP2 (Ptgdr2) forward: 5′- CGATGCTCCTGCTGCTTATC -3′
EP2 (Ptgdr2) reverse: 5′- TGCATGCGAATGAGGTTGAG -3′
EP3 (Ptgdr3) forward: 5′- GGGATCATGTGTGTGCTGTC -3′
EP3 (Ptgdr3) reverse: 5′- GCATTGCTCAACCGACATCT -3′
EP4 (Ptgdr4) forward: 5′- TCTCTGGTGGTGCTCATCTG -3′
EP4 (Ptgdr4) reverse: 5′- GTCTTTCACCACGTTTGGCT -3′

2.9. Computational analysis of protein-protein interaction

The electrostatic energy of interaction between the two proteins was calculated solving the linear Poisson–Boltzmann equation. To this end, the software Adaptive Poisson-Boltzmann Solver (APBS) [27] was utilized. This software was used to calculate the electrostatic energy of each individual structure and of the complex formed by the two proteins. Then, by calculating the difference between the complex and the individual structures (Eq. (1)), electrostatic interaction energy was found.

$$E_{Interaction} = E_{Complex} - (E_{Protein\ 1} + E_{Protein\ 2}) \quad (1)$$

This procedure was carried over the various possible orientations that the proteins can adopt between each other. To be able to sample all the possible configurations, an own-developed program was used. This program generates all the necessary configurations by rotating the two proteins around each other. First protein 1 was rotated around protein 2 so that protein 1 covered all possible positions along an imaginary sphere around protein 2. Then, protein 1 was rotated around its own center, in such a way that all possible orientations were sampled. Finally, the distance (**r**) between each final structure was set equal. This distance was calculated by projecting all the coordinates of the two structures to the axis defined by the center of both structures. Then, the minimum distance

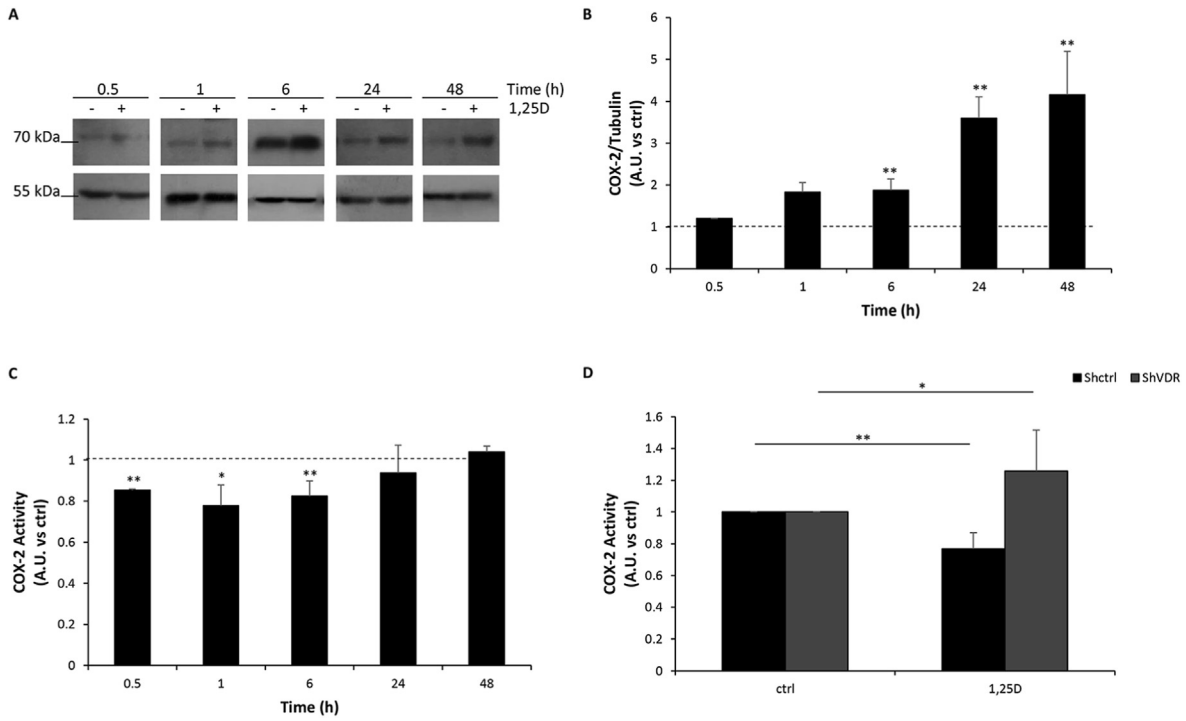

Figure 3. ***1α,25(OH)$_2$D$_3$ increases COX-2 protein levels whereas decreases its activity on a VDR dependent manner***. vGPCR cells were treated with 1α,25(OH)$_2$D$_3$ (10 nM) or vehicle (0.01% ethanol) for different times (0.5–48 h) (A), (B) and (C). Stable vGPCR cells vGPCR-shVDR or control shRNA (vGPCR-shctrl) were treated with 1α,25(OH)$_2$D$_3$ (10 nM) or vehicle (0.01% ethanol) for 30 min (D). Cell lysates were subject to Western blot analysis with anti-COX-2 and anti-tubulin antibodies. The representative blots are presented (A). The quantification of protein bands by densitometry was represented as the ratio between COX-2/Tubulin referred to control in bar graphs (B). Peroxidase activity was measured colorimetrically with COX-2 Activity Assay kit (C) and (D). Statistical significance from at least three independent experiments was evaluated using Student's t-test (**$p < 0.01$, *$p < 0.05$) (B) and (C). Differences between ctrl and treated conditions in vGPCR-shctrl or -shVDR group and between treated conditions in vGPCR-shctrl and -shVDR group were analyzed by Student's t-test (**$p < 0.01$, *$p < 0.05$).

between the two structures over this axis was set to the desired value of **r** = 10 Å. The program was written in Python and needs the structure of both proteins in pqr format, which contains electric charge and Van der Waals radius for each atom.

With that goal, reported pdb structures from two different species, including Rat and Mouse were extracted from the PDBDataBank [28] (PDB IDs: 1RJK and 3QMO), while unreported tertiary structure proteins were modeled with homology model methods by funneling their primary sequences through Swiss Model server [29, 30, 31, 32, 33] (Table 1). Then, PDB2PQR [34] was used to obtain pqr files from pdb files. Finally, the user must define the distance between the final orientations **r**, and the size of the angular steps used when rotating. In this case all angular steps where set to 45° and **r** = 10 Å.

2.10. Statistical analysis

Results presented as means ± SD, were analyzed by one-way ANOVA followed by Bonferroni test or two-tailed t-test to assess differences between control (vehicle) and treated (1α,25(OH)$_2$D$_3$) conditions at each time (*$p < 0.05$ or **$p < 0.01$).

3. Results

3.1. Celecoxib reduces vGPCR cell number and viability

Previously we have demonstrated that 1α,25(OH)$_2$D$_3$ has anti-proliferative effects on the growth of vGPCR cells [21]. Given that COX-2 expression is induced by vGPCR, we researched if COX-2 regulation contributed to the inhibitory effect of 1α,25(OH)$_2$D$_3$. Proliferation assays were analyzed by counting vGPCR cells in Neubauer chamber after treatment with, 1α,25(OH)$_2$D$_3$ (10 nM) or vehicle (0.01% ethanol) or Celecoxib (10–20 μM) in DMEM 2% fetal bovine serum (FBS) for 48 h. Cellular morphological changes were observed by light field microscopy. Cell viability was measured using the CellTiter 96® AQ$_{ueous}$ One Solution Cell Proliferation Assay containing 3-(4,5-dimethylthiazol-2-yl)-5-(3-carboxymethoxyphenyl)-2-(4 sulfophenyl)-2H-tetrazolium, inner salt (MTS). Results in Figure 1A and B show that similar to 1α,25(OH)$_2$D$_3$, COX-2 inhibitor Celecoxib decreased vGPCR cell number significantly in a dose-dependent manner, presenting through the micrographs abnormal shrinking and rounding, typical apoptotic alterations. Results in Figure 1C indicate that cell viability was diminished by 1α,25(OH)$_2$D$_3$ or Celecoxib (10 μM) and no further effect was observed when both agents were used in combination.

3.2. Cox-2 mRNA is up-regulated by 1α,25(OH)$_2$D$_3$ in a VDR dependent mechanism

There are many reports showing the anti-inflammatory action of 1α,25(OH)$_2$D$_3$ through the inhibition of COX-2 expression [20, 35, 36]. On the other hand, some data demonstrated vitamin D induces COX-2 expression in epithelial cells [37, 38] Therefore *Cox*-2 mRNA levels were evaluated by qRT-PCR at different time points (0.3–48 h) after 1α,25(OH)$_2$D$_3$ (10 nM) or vehicle (0.01% ethanol) treatments in presence of DMEM 2% FBS. Results presented in Figure 2A show an increased expression of *Cox*-2 mRNA induced by 1α,25(OH)$_2$D$_3$. To evaluate if this rise was dependent of VDR, vGPCR cells targeted with small hairpin RNA against mouse VDR (vGPCR-shVDR) or control shRNA (vGPCR-shctrl) were treated with 1α,25(OH)$_2$D$_3$ (10 nM) or vehicle (0.01% ethanol) in presence of DMEM 2% FBS for 24 h. Effectively, the increase in COX-2 mRNA expression after 1α,25(OH)$_2$D$_3$ treatment was VDR dependent (Figure 2B).

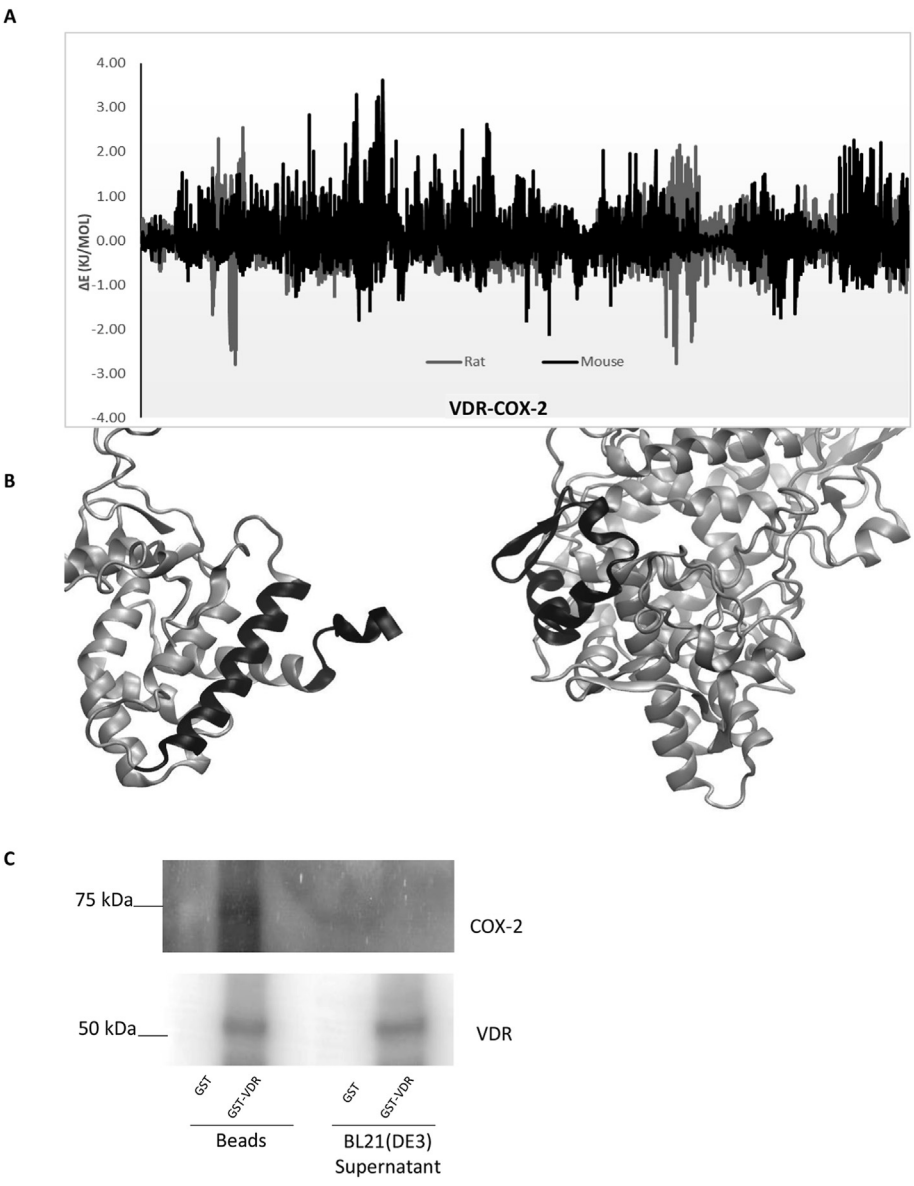

Figure 4. ***COX-2 and VDR interaction.*** Computational analysis of protein-protein interaction is shown. Electrostatic energy versus different configurations of VDR–COX2 complex. 3872 relative positions were evaluated. The starting point is a random position, but always the same. For clarity, angles degree variations were no labeled. Curves with different colors indicate VDR–COX2 complex from different species. Grey for Rat and black for Mouse (A). View of Mouse VDR-COX2 complex in the configuration of minimum energy. Left in black: putative mouse VDR leading regions. Right in black: putative mouse COX2 leading regions (B). Protein content from vGPCR cell lysates was incubated with BL21 pellet containing glutathione-Sepharose beads plus GST or GST-VDR. After centrifugation beads were eluted with loading buffer for Western blot assay with anti-COX-2 and anti-VDR antibodies. Representative blots from three experiments are shown (C).

3.3. 1α,25(OH)$_2$D$_3$ regulates COX-2 protein levels and activity

To further characterize COX-2 regulation by 1α,25(OH)$_2$D$_3$, we investigated COX-2 protein levels using Western blot. vGPCR cells were treated with 1α,25(OH)$_2$D$_3$ (10 nM) or vehicle (0.01% ethanol) in DMEM 2% fetal bovine serum (FBS) for different times (0.5–48 h). The results in Figure 3A show representative blots of a significant increase in COX-2 expression after treatment from 6 h onwards. Figure 3B shows the quantification of the bands from at least three independent experiments. Next, the regulation on COX-2 activity was investigated. vGPCR cells were treated with 1α,25(OH)$_2$D$_3$ (10 nM) or vehicle (0.01% ethanol) in DMEM 2% fetal bovine serum (FBS) for different times (0.5–48 h). Peroxidase activity was measured colorimetrically with a COX-2 Activity Assay kit (Cayman N° 760151). The results in Figure 3C indicate that COX-2 activity was rapidly but transiently reduced by 1α,25(OH)$_2$D$_3$ treatment and stabilized at longer periods. To evaluate a connection between VDR and the reduced activity of COX-2 enzyme, a VDR knockdown cellular model was used to measure COX-2 activity at one of the time points where its activity was significantly reduced. vGPCR cells, vGPCR-shVDR or control shRNA (vGPCR-shctrl), were incubated with 1α,25(OH)$_2$D$_3$ (10 nM) or vehicle (0.01% ethanol) in DMEM 2% FBS for 30 min. Results presented in Figure 3D demonstrate that COX-2 activity is higher in treated conditions were VDR is knockdown, hence reduced activity after 1α,25(OH)$_2$D$_3$ treatment depends on VDR.

3.4. VDR interacts with COX-2

Although COX-2 gene and protein levels are increased after 1α,25(OH)$_2$D$_3$ treatment, the enzymatic activity decreases rapidly in a VDR-dependent manner. Therefore, to elucidate how these events are linked, we tested the hypothesis of a potential VDR and COX-2 interaction. We first examined by *in silico* studies the electrostatic energy of the potential binding between VDR and COX-2 in two different species. For rat VDR-COX-2 interaction, the electrostatic energy landscape showed grouped significant minimum values as expected in a favorable interaction for this method [39, 40, 41]. In this case, Lys123-GLU127 and ALA345-PRO368 residues from VDR seem to lead the orientation in the interaction by pointing to the GLU402-ARG414 and SER552- GLN569 regions of COX-2. For mouse VDR-COX-2 interaction, some appreciable minimum values were found, although they were not as clustered nor as marked as for rat VDR-COX-2 interaction. Similar to the rat electrostatic interaction landscape, minimum values occurred for relative positions in

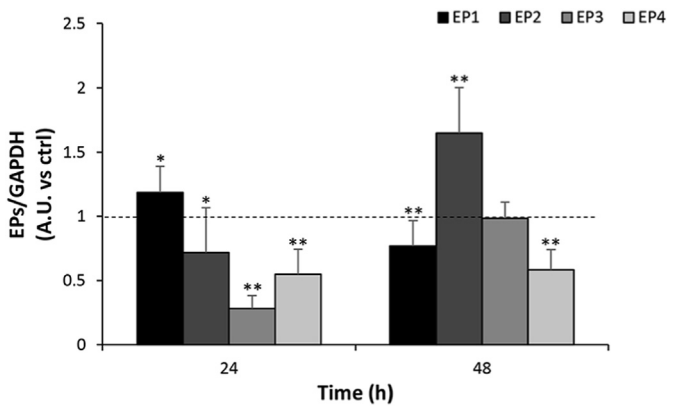

Figure 5. ***EPs mRNA expression is regulated by 1α,25(OH)$_2$D$_3$.*** vGPCR cells were incubated with 1α,25(OH)$_2$D$_3$ (10 nM) or vehicle (0.01% ethanol) in DMEM 2% FBS for 24–48 h. 1 μg of total RNA was extracted, and reverse transcribed. qRT-PCR was used to analyze gene expression of *EP1*, *EP2*, *EP3*, *EP4* and *Gapdh*. Results are expressed as a ratio between treated and vehicle conditions normalized to *Gapdh* mRNA levels. The statistical significance of data from at least three independent experiments was analyzed by Student's t-test (**$p < 0.01$, *$p < 0.05$).

which LEU116-GLU127 and ASP343-ARG365 residues from VDR seemingly lead the orientation in the interaction by pointing towards the THR394-GLN429 region of COX-2 (Figure 4A). To confirm these data, we evaluated a possible interaction among VDR and COX-2 by GST-pull-down assay. Total lysates from vGPCR cells were incubated with GST-VDR or GST glutathione-Sepharose beads obtained from previously transformed *E. coli* BL21, respectively. To determine VDR/COX-2 interaction after incubation proteins were analyzed by Western Blot. As shown in Figure 4C, COX-2 co-precipitates with GST-VDR. These results argue in favor of an interaction between COX-2 and VDR.

3.5. 1α,25(OH)$_2$D$_3$ regulates EPs mRNA expression

The COX-2 dysregulation leads to elevated levels of PGE$_2$, which acts locally in an autocrine or paracrine manner through four pharmacologically distinct G-protein coupled plasma membrane receptors, EP1, EP2, EP3 and EP4. Each one can activate different downstream signaling pathways [14]. To investigate if 1α,25(OH)$_2$D$_3$ changes the expression levels of EPs receptors when COX-2 activity turns to stable levels, vGPCR cells were incubated with 1α,25(OH)$_2$D$_3$ (10 nM) or vehicle (0.01% ethanol) in DMEM 2% FBS for 24–48 h. Total RNA was isolated and reverse transcribed followed by qRT-PCR using specific primers to detect *EP1*, *EP2*, *EP3* and *EP4* mRNA levels and *Gapdh* mRNA was used to normalize gene expression. The results presented in Figure 5 indicate that high-affinity receptors *EP3* and *EP4* are down-regulated; nevertheless, *EP1* and *EP2* low-affinity receptors behave differently. *EP1* diminishes it expression at 48 h but *EP2* mRNA levels are higher. These results present a differential suppression of PGE$_2$ biological activity by 1α,25(OH)$_2$D$_3$.

4. Discussion

1α,25(OH)$_2$D$_3$, the biologically-active form of vitamin D, exerts antiproliferative and pro-differentiating actions on cancer cells [20]. Most of its actions depend on VDR [17]. There is evidence that 1α, 25(OH)$_2$D$_3$ has anti-inflammatory effects through the inhibition of COX-2 expression [35, 36]. COX or prostaglandin-endoperoxide synthase is the enzyme that catalyzes the conversion of arachidonic acid (AA) into prostaglandin H2, which is converted into proinflammatory lipid metabolites like PGE$_2$, an inflammation-activating agent [8, 42].

Since COX-2 plays a key role in prostanoids production and inflammation, and is highly activated by vGPCR in Kaposi's sarcoma [7], it raises the question whether the antiproliferative effects of 1α,25(OH)$_2$D$_3$ on vGPCR could be caused in part to COX-2 down-regulation. Our findings demonstrated that the inhibition of COX-2 with Celecoxib reduced the proliferation of endothelial cells transformed by vGPCR like 1α, 25(OH)$_2$D$_3$ (Figure 1). As no additive effect was observed when both agents were incorporated together, it implies that the hormone and Celecoxib could act by the same mechanism. However, time response studies showed COX-2 mRNA and protein levels increased after 1α, 25(OH)$_2$D$_3$ treatment (Figures 2A and 3A), moreover, this expression rise was VDR dependent (Figure 2B). Consequently, we measured the peroxidase activity of COX-2 in vGPCR cells and we found a low activity after 1α,25(OH)$_2$D$_3$ treatment for short periods of time that stabilized itself later (Figure 3B). This effect was VDR-dependent (Figure 3C) indicating a connection between COX-2 and VDR responsible for this high expression with diminished activity. Regarding to the electrostatic interaction results, even though the unavailability of a complete tridimensional structure for two of the proteins studied showed not conclusive interactions between VDR and COX-2, the performed test was informative. According to the results obtained from the electrostatic analyses from rat and mouse VDR-COX-2 interactions, similar regions of these proteins could be involved in leading the interaction (Figure 4A and B). Next, GST-Pull Down results exposed an interaction between COX-2 and VDR that supported the previous electrostatic analysis (Figure 4C) and provided evidence for an interaction between COX-2 and VDR. While COX-2 is generally expressed in the cytoplasm, studies have indicated perinuclear localization [43] and trafficking between the nucleus and the cytoplasm in endothelial cells [44] affecting nuclear events, data that supports the plausibility of an interaction between COX-2 and VDR in intact cells.

On the other hand, one of the main products of COX-2 catalyzed reactions is PGE$_2$, which performs its inflammatory actions through four G-protein couple receptors. Each of these EPs receptors can activate different downstream signaling pathways making PGE$_2$ able to mediate highly varied effects on different types of cells [14]. Previous reports indicated that COX-2 increases PGE2 production in HUVEC cells expressing vGPCR [7]. Moreover, 1α,25(OH)$_2$D$_3$ decreases PGE2 secretion and represses EPs mRNA expression in prostate cancer cells, regulating PGs metabolism and biological actions [45]. In this work, we showed that high-affinity receptors EP3 and EP4 are down regulated after 1α,25(OH)$_2$D$_3$ treatment, on the contrary, EP1 and EP2 low-affinity receptors which require significantly higher levels of PGE$_2$ for activation behave differently. EP1 diminishes it expression at 48 h but EP2 mRNA levels are higher (Figure 5). Both the EP2 and EP4 receptors are connected to G-stimulatory (Gαs) proteins, which through adenylate cyclase activation increase cAMP cell levels that leads to the activation of PKA or the GSK3β/β-catenin pathway. Consequently, despite being linked to the same G protein, the different affinity to PGE$_2$ shows a differential suppression for EPs receptors' expression. There are reports of an autocrine PGE2 positive feedback involving EP2 and EP4 to induce COX-2 production [46, 47], this reinforced mechanism due to the diminish production of PGE2 could explain COX-2 low activity with a high expression.

In conclusion, despite more studies are needed to elucidate the effect of 1α,25(OH)$_2$D$_3$ in PGE2 biological activity, these results demonstrate that 1α,25(OH)$_2$D$_3$ antiproliferative effects on vGPCR cells could be caused by a down regulation of PGE$_2$ production through the interaction between VDR and COX-2 and a differential suppression of EPs receptors expression.

Declarations

Author contribution statement

V.G. Pardo: Conceived and designed the experiments; Analyzed and interpreted the data; Contributed reagents, materials, analysis tools or data; Wrote the paper.

C. Tapia and G.A. Salvador: Performed the experiments; Analyzed and interpreted the data; Wrote the paper.

F. Zamarreño, J. Viso and C.I. Casali: Performed the experiments.

M. del Carmen Fernández:Contributed reagents, materials, analysis tools or data.

J.H. White: Conceived and designed the experiments; Contributed reagents, materials, analysis tools or data.

Funding statement

This work was supported by grants from Agencia Nacional de Promoción Científica y Tecnológica (ANPCYT, PICT 2013-0562), Consejo Nacional de Investigaciones Científicas y Tecnológicas (CONICET, PIP1122011010040), Universidad Nacional del Sur (24/ZB68) to Verónica González Pardo.

Competing interest statement

The authors declare no conflict of interest.

Additional information

No additional information is available for this paper.

References

[1] C. Ethel, B. Damania, E.K. Susan, M. Jeffrey, B. Mark, D. Whitby, Kaposi sarcoma, Nat. Rev. Dis. Prim. 5 (2019) 1–21.
[2] D. Martin, J.S. Gutkind, Kaposi's sarcoma virally encoded, G-protein-coupled receptor: a paradigm for paracrine transformation, Methods Enzymol. 460 (2009) 125–150.
[3] E.A. Mesri, E. Cesarman, C. Boshoff, Kaposi's sarcoma and its associated herpesvirus, Nat. Rev. Canc. 10 (2010) 707–719.
[4] S. Montaner, A. Sodhi, A. Molinolo, T.H. Bugge, E.T. Sawai, Y. He, Y. Li, P.E. Ray, J.S. Gutkind, Endothelial infection with KSHV genes in vivo reveals that vGPCR initiates Kaposi's sarcomagenesis and can promote the tumorigenic potential of viral latent genes, Canc. Cell 3 (2003) 23–36.
[5] N. Sharma-Walia, H. Raghu, S. Sadagopan, R. Sivakumar, M.V. Veettil, P.P. Naranatt, M.M. Smith, B. Chandran, Cyclooxygenase 2 induced by Kaposi's sarcoma-associated herpesvirus early during in vitro infection of target cells plays a role in the maintenance of latent viral gene expression, J. Virol. 80 (2006) 6534–6552.
[6] P.P. Naranatt, H.H. Krishnan, S.R. Svojanovsky, C. Bloomer, S. Mathur, B. Chandran, Host gene induction and transcriptional reprogramming in Kaposi's sarcoma-associated herpesvirus (KSHV/HHV-8)-Infected endothelial, fibroblast, and B cells: insights into modulation events early during infection, Cancer Res. 64 (2004) 72–84.
[7] B.D. Shelby, H.L. LaMarca, H.E. McFerrin, A.B. Nelson, J.A. Lasky, G. Sun, L. Myatt, M.K. Offermann, C.A. Morris, D.E. Sullivan, Kaposi's sarcoma associated herpesvirus G-protein coupled receptor activation of cyclooxygenase-2 in vascular endothelial cells, Virol. J. 4 (2007) 1–9.
[8] T. Cordes, F. Hoellen, C. Dittmer, D. Salehin, S. Kümmel, M. Friedrich, F. Köster, S. Becker, K. Diedrich, M. Thill, Correlation of prostaglandin metabolizing enzymes and serum PGE 2 levels with vitamin D receptor and serum 25(OH) 2D 3 levels in breast and ovarian cancer, Anticancer Res. 32 (2012) 351–357.
[9] N. Sharma-Walia, A.G. Paul, V. Bottero, S. Sadagopan, M.V. Veettil, N. Kerur, B. Chandran, Kaposi's Sarcoma Associated Herpes Virus (KSHV) induced COX-2: a key factor in latency, inflammation, angiogenesis, cell survival and invasion, PLoS Pathog. 6 (2010).
[10] W.L. Smith, D.L. Dewitt, R.M. Garavito, C. Yclooxygenases, Structural , cellular , and molecular biology, Annu. Rev. Biochem. 69 (2000) 145–182.
[11] D.T. Lin, K. Subbaramaiah, J.P. Shah, A.J. Dannenberg, J.O. Boyle, Cyclooxygenase-2: a novel molecular target for the prevention and treatment of head and neck cancer, Head Neck 24 (2002) 792–799.
[12] A.J. Dannenberg, K. Subbaramaiah, Targeting cyclooxygenase-2 in human neoplasia: rationale and promise, Canc. Cell 4 (2003) 431–436.
[13] J.E. Rundhaug, M.S. Simper, I. Surh, S.M. Fischer, The role of the EP receptors for prostaglandin E2 in skin and skin cancer, Canc. Metastasis Rev. 30 (2011) 465–480.
[14] G. O'Callaghan, A. Houston, Prostaglandin E2 and the EP receptors in malignancy: possible therapeutic targets? Br. J. Pharmacol. 172 (2015) 5239–5250.
[15] K.K. Deeb, D.L. Trump, C.S. Johnson, Vitamin D signalling pathways in cancer: potential for anticancer therapeutics, Nat. Rev. Canc. 7 (2007) 684–700.
[16] I. Martínez-Reza, L. Díaz, D. Barrera, M. Segovia-Mendoza, S. Pedraza-Sánchez, G. Soca-Chafre, F. Larrea, R. García-Becerra, Calcitriol inhibits the proliferation of triple-negative breast cancer cells through a mechanism involving the proinflammatory cytokines IL-1β and TNF-α, J. Immunol. Res. 2019 (2019).
[17] A.V. Krishnan, D. Feldman, Mechanisms of the anti-cancer and anti-inflammatory actions of vitamin D, Annu. Rev. Pharmacol. Toxicol. 51 (2011) 311–336.
[18] V. González Pardo, N. D'Elia, A. Verstuyf, R. Boland, A. Russo de Boland, NFκB pathway is down-regulated by 1α,25(OH)(2)-vitamin D(3) in endothelial cells transformed by Kaposi sarcoma-associated herpes virus G protein coupled receptor, Steroids 77 (2012) 1025–1032.
[19] V. González Pardo, A. Verstuyf, R. Boland, A. Russo de Boland, Vitamin D analogue TX 527 down-regulates the NF-κB pathway and controls the proliferation of endothelial cells transformed by Kaposi sarcoma herpesvirus, Br. J. Pharmacol. 169 (2013) 1635–1645.
[20] M. Thill, A. Woeste, K. Reichert, D. Fischer, A. Rody, M. Friedrich, F. Köster, Vitamin D inhibits ovarian cancer cell line proliferation in combination with celecoxib and suppresses cyclooxygenase-2 expression, Anticancer Res. 35 (2015) 1197–1203.
[21] V. González Pardo, D. Martin, J.S. Gutkind, A. Verstuyf, R. Bouillon, A.R. de Boland, R.L. Boland, 1α,25-dihydroxyvitamin D3 and its TX527 analog inhibit the growth of endothelial cells transformed by Kaposi sarcoma-associated herpes virus G protein-coupled receptor in vitro and in vivo, Endocrinology 151 (2010) 23–31.
[22] V. González Pardo, R. Boland, A.R. de Boland, 1alpha,25(OH)(2)-Vitamin D(3) stimulates intestinal cell p38 MAPK activity and increases c-Fos expression, Int. J. Biochem. Cell Biol. 38 (2006) 1181–1190.
[23] C. Solomon, M. Macoritto, X.L. Gao, J.H. White, R. Kremer, The unique tryptophan residue of the vitamin D receptor is critical for ligand binding and transcriptional activation, J. Bone Miner. Res. 16 (2001) 39–45.
[24] B.-S. An, L.E. Tavera-Mendoza, V. Dimitrov, X. Wang, M.R. Calderon, H.-J. Wang, J.H. White, Stimulation of sirt1-regulated FoxO protein function by the ligand-bound vitamin D receptor, Mol. Cell Biol. 30 (2010) 4890–4900.
[25] R. Salehi-Tabar, B. Memari, H. Wong, V. Dimitrov, N. Rochel, J.H. White, The tumor suppressor Fbw7 and the Vitamin D receptor are mutual cofactors in protein turnover and transcriptional regulation, Mol. Canc. Res. 17 (2019) 709–719.
[26] A. Suares, M. Mori Sequeiros Garcia, C. Paz, V. González Pardo, Antiproliferative effects of Bortezomib in endothelial cells transformed by viral G protein-coupled receptor associated to Kaposi's sarcoma, Cell. Signal. 32 (2017) 124–132.
[27] E. Jurrus, D. Engel, K. Star, K. Monson, J. Brandi, L.E. Felberg, D.H. Brookes, L. Wilson, J. Chen, K. Liles, M. Chun, P. Li, D.W. Gohara, T. Dolinsky, R. Konecny, D.R. Koes, J.E. Nielsen, T. Head-Gordon, W. Geng, R. Krasny, G.W. Wei, M.J. Holst, J.A. McCammon, N.A. Baker, Improvements to the APBS biomolecular solvation software suite, Protein Sci. 27 (2018) 112–128.
[28] H.M. Berman, J.D. Westbrook, Z. Feng, G.L. Gilliland, T.N. Bhat, H. Weissig, I.N. Shindyalov, P.E. Bourne, The protein data bank, Nucleic Acids Res. 28 (2000) 235–242.
[29] A. Waterhouse, M. Bertoni, S. Bienert, G. Studer, G. Tauriello, R. Gumienny, F.T. Heer, T.A.P. De Beer, C. Rempfer, L. Bordoli, R. Lepore, T. Schwede, SWISS-MODEL: homology modelling of protein structures and complexes, Nucleic Acids Res. 46 (2018) W296–W303.
[30] S. Bienert, A. Waterhouse, T.A.P. De Beer, G. Tauriello, G. Studer, L. Bordoli, T. Schwede, The SWISS-MODEL Repository-new features and functionality, Nucleic Acids Res. 45 (2017) D313–D319.
[31] N. Guex, M.C. Peitsch, T. Schwede, Automated comparative protein structure modeling with SWISS-MODEL and Swiss-PdbViewer: a historical perspective, Electrophoresis 30 (2009) 162–173.
[32] P. Benkert, M. Biasini, T. Schwede, Toward the estimation of the absolute quality of individual protein structure models, Bioinformatics 27 (2011) 343–350.
[33] M. Bertoni, F. Kiefer, M. Biasini, L. Bordoli, T. Schwede, Modeling protein quaternary structure of homo- and hetero-oligomers beyond binary interactions by homology, Sci. Rep. 7 (2017) 1–15.
[34] T.J. Dolinsky, P. Czodrowski, H. Li, J.E. Nielsen, J.H. Jensen, G. Klebe, N.A. Baker, PDB2PQR: expanding and upgrading automated preparation of biomolecular structures for molecular simulations, Nucleic Acids Res. 35 (2007) 522–525.
[35] A.V. Krishnan, S. Swami, D. Feldman, Vitamin D and breast cancer: inhibition of estrogen synthesis and signaling, J. Steroid Biochem. Mol. Biol. 121 (2010) 343–348.
[36] Q. Wang, Y. He, Y. Shen, Q. Zhang, D. Chen, C. Zuo, J. Qin, H. Wang, J. Wang, Y. Yu, Vitamin D inhibits cox-2 expression and inflammatory response by targeting thioesterase superfamily member 4, J. Biol. Chem. 289 (2014) 11681–11694.
[37] A. Ravid, O. Shenker, E. Buchner-Maman, C. Rotem, R. Koren, Vitamin D induces cyclooxygenase 2 dependent prostaglandin E2 synthesis in HaCaT keratinocytes, J. Cell. Physiol. 231 (2016) 837–843.
[38] R. Lin, Y. Nagai, R. Sladek, Y. Bastien, J. Ho, K. Petrecca, G. Sotiropoulou, E.P. Diamandis, T.J. Hudson, J.H. White, Expression profiling in squamous carcinoma cells reveals pleiotropic effects of vitamin D3 analog EB1089 signaling on cell proliferation, differentiation, and immune system regulation, Mol. Endocrinol. 16 (2002) 1243–1256.
[39] D.F. Vallejo, F. Zamarreño, D.M.A. Guérin, J.R. Grigera, M.D. Costabel, Prediction of the most favorable configuration in the ACBP-membrane interaction based on electrostatic calculations, Biochim. Biophys. Acta Biomembr. 1788 (2009) 696–700.
[40] F. Zamarreño, F.E. Herrera, B. Córsico, M.D. Costabel, Similar structures but different mechanisms: prediction of FABPs-membrane interaction by electrostatic calculation, Biochim. Biophys. Acta Biomembr. 1818 (2012) 1691–1697.
[41] F. Zamarreño, A. Giorgetti, M.J. Amundarain, J.F. Viso, B. Córsico, M.D. Costabel, Conserved charged amino acids are key determinants for fatty acid binding proteins (FABPs)-membrane interactions. A multi-methodological computational approach, J. Biomol. Struct. Dyn. 36 (2017) 861–877.
[42] A.G. Paul, B. Chandran, N. Sharma-Walia, Cyclooxygenase-2-prostaglandin e2-eicosanoid receptor inflammatory axis: a key player in Kaposi's sarcoma-associated herpes virus associated malignancies, Transl. Res. 162 (2013) 77–92.

[43] R. Thanan, M. Murata, N. Ma, O. Hammam, M. Wishahi, T. El Leithy, Y. Hiraku, S. Oikawa, S. Kawanishi, Nuclear localization of COX-2 in relation to the expression of stemness markers in urinary bladder cancer, Mediat. Inflamm. 2012 (2012).
[44] H. Parfenova, V.N. Parfenov, B.V. Shlopov, V. Levine, S. Falkos, M. Pourcyrous, C.W. Leffler, Dynamics of nuclear localization sites for COX-2 in vascular endothelial cells, Am. J. Physiol. Cell Physiol. 281 (2001) 166–178.
[45] J. Moreno, A.V. Krishnan, S. Swami, L. Nonn, D.M. Peehl, D. Feldman, Regulation of prostaglandin metabolism by calcitriol attenuates growth stimulation in prostate cancer cells, Cancer Res. 65 (2005) 7917–7925.
[46] D.A. Bradbury, R. Newton, Y.M. Zhu, H. El-Haroun, L. Corbett, A.J. Knox, Cyclooxygenase-2 induction by bradykinin in human pulmonary artery smooth muscle cells is mediated by the cyclic AMP response element through a novel autocrine loop involving endogenous prostaglandin E2, E-prostanoid 2 (EP2), and EP4 receptors, J. Biol. Chem. 278 (2003) 49954–49964.
[47] M.D. Díaz-Muñoz, I.C. Osma-García, M. Fresno, M.A. Iñiguez, Involvement of PGE 2and the cAMP signalling pathway in the up-regulation of COX-2 and mPGES-1 expression in LPS-activated macrophages, Biochem. J. 443 (2012) 451–461.